Food Chemistry 491 (2025) 145247

Contents lists available at ScienceDirect

Food Chemistry

journal homepage: www.elsevier.com/locate/foodchem

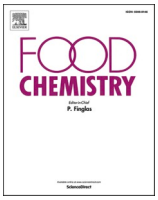

Enhancing cyclodextrin glycosyltransferase-mediated potato starch modification via plasma-activated water and twin-screw extrusion treatment

Fanglei Zou [a], Hongyun Hao [a], Miao Yang [a], Chunming Tan [b], Lin Chen [c], Junhua Wu [a], Hongying Wang [a,*]

[a] College of Engineering, China Agricultural University, Beijing 100083, China
[b] National R&D Center for Freshwater Fish Processing, College of Life Sciences, Jiangxi Normal University, Nanchang, Jiangxi 330022, China
[c] School of Chemistry, Chemical Engineering and Biotechnology, Nanyang Technological University, Singapore 637459, Singapore

ARTICLE INFO

Keywords:
Potato starch
Plasma-activated water
Extrusion
Structure
Rheological properties
In vitro digestibility

ABSTRACT

This study investigated the effects of plasma-activated water (PAW), extrusion, and their combination on the physicochemical, rheological, and digestive properties of potato starch during cyclodextrin glycosyltransferase (CGTase)-mediated modification. All treatments decreased the molecular weight and amylopectin chain length. Differential scanning calorimetry results showed PAW treatment increased the gelatinization enthalpy of potato starch from 12.61 J/g to 15.66 J/g and increased its gelatinization temperatures compared with native starch. Low-field nuclear magnetic resonance results indicated both PAW and extrusion treatments altered water distribution, promoting the conversion of free and weakly bound water to tightly bound states. Rheological tests indicated the combined PAW, extrusion, and CGTase treatment (EACG) yielded starch gel with the highest elastic and viscous moduli. Furthermore, EACG modification enhanced the solubility and increased the resistant starch content from 31.69 % to 61.38 %. This study developed a novel green method for modulating potato starch properties, with potential applications such as low-glycemic index food ingredients and gelling agents.

1. Introduction

Potato starch is widely used in food and non-food industries due to its excellent thickening, binding, gelling, and encapsulation properties (Mahmood et al., 2017). However, native starch suffers from several limitations, such as poor solubility, high retrogradation tendency, and limited film-forming capacity, which restricts its functionality in targeted applications. As a result, various modification techniques are employed to enhance its functional properties and expand its potential uses. To overcome these limitations, various starch modification methods have been developed, including physical, chemical, and enzymatic approaches. Among them, enzymatic modification is valued for its selectivity, while physical techniques such as extrusion and cold plasma are gaining attention for their green and scalable characteristics (Ji et al., 2021; Román et al., 2016; Zou et al., 2025).

Cyclodextrin glycosyltransferase (CGTase), a member of the glycoside hydrolase family, catalyzes partial starch hydrolysis by cleaving α-1,4-glycosidic bonds and transfers the resulting fragments to form cyclodextrins (CDs) through a transglycosylation reaction. CGTase slows starch retrogradation and aging in starch-based products by modifying

Abbreviations: NPS, Native starch; ETN, Twin-screw extruded starch; NPPA, NPS mixed with PAW; ETPA, ETN mixed with PAW; NPCG, NPS treated with CGTase; ETCG, ETN treated with CGTase; NACG, NPS sequentially treated with PAW and CGTase; EACG, ETN sequentially treated with PAW and CGTase; PAW, Plasma-activated water; CGTase, Cyclodextrin glycosyltransferase; RDS, Rapidly digestible starch; SDS, Slowly digestible starch; RS, Resistant starch; CDs, Cyclodextrins; CP, Cold plasma; ORP, Oxidation-reduction potential; EC, Electrical conductivity; ROS, Reactive oxygen species; GOPOD, Glucose oxidase-peroxidase; DW, Distilled water; CLD, Chain length distribution; M_w, Weight-average molecular weight; M_n, Number-average molecular weight; RI, Refractive index; XRD, X-ray diffraction; RC, Relative crystallinity; HPLC, High-performance liquid chromatography; SEM, Scanning electron microscopy; CLSM, Confocal laser scanning microscopy; PLM, Polarized light microscopy; TGA, Thermogravimetric analysis; LVR, linear viscoelastic region; LAOS, Large-amplitude oscillatory shear; DP, Degree of polymerization; PDI, polydispersity index..

* Corresponding author at: College of Engineering, China Agricultural University, Beijing 100083, China.
E-mail address: hongyingw@cau.edu.cn (H. Wang).

https://doi.org/10.1016/j.foodchem.2025.145247
Received 9 December 2024; Received in revised form 8 June 2025; Accepted 19 June 2025
Available online 20 June 2025

the starch structure, thereby enhancing the quality and shelf life of baked goods, as well as increasing the levels of slowly digestible starch (SDS) and resistant starch (RS) (Ji et al., 2021). CDs are cyclic oligosaccharides linked by α-1,4-glycosidic bonds, commonly including α-CD, β-CD, and γ-CD. CDs have a hydrophilic exterior and a hydrophobic interior, allowing guest molecules to be embedded within their hydrophobic cavity through van der Waals forces (Ma et al., 2023). CDs enable controlled release, increased solubility of guest molecules, improved odor, and protection of sensitive food components. Therefore, CDs show a wide range of potential applications in food (López-Nicolás & García-Carmona, 2007) and packaging (López-de-Dicastillo et al., 2010).

Cold plasma (CP) consists of electrons, ions, ultraviolet radiation, free radicals, and excited molecules. Plasma-activated water (PAW) is a liquid produced by CP interacting with water, characterized by high oxidation-reduction potential (ORP), high electrical conductivity (EC), and low pH. It contains reactive oxygen species (ROS) (Zou et al., 2025). Chou et al. (2023) found that PAW treatment improved the solubility, gel hardness, thermal stability, and reduced retrogradation of potato starch. Despite its potential (Han et al., 2023; Zou, Shinali, et al., 2024), few studies have explored the effects of PAW combined with other technologies on starches.

Extrusion is a common starch modification method that applies high pressure and mechanical energy to shear, heat, and shape starch. It alters the structure, physicochemical properties, and digestibility of starch, improving solubility and enzymatic hydrolysis rate, thus increasing its industrial applicability (Sun et al., 2021). The degree of modification influences the rheological properties, gelatinization behavior, and final product quality (Roman et al., 2018). However, the effects and mechanisms of combining PAW and twin-screw extrusion on CGTase-mediated modified potato starch remain underexplored.

Numerous studies have reported the effectiveness of single treatments using ETN, PAW, and CGTase in modifying the structure and physicochemical properties (such as solubility, gel strength, thermal performance, and digestibility) of starch. However, the use of synergistic multiple modification strategies may hold greater potential. The primary aim of this study is to systematically evaluate the impact of PAW and ETN on CGTase-mediated potato starch modification, focusing on the structural, physicochemical, rheological, and digestive properties following extrusion. We hypothesized that the synergistic integration of PAW treatment and twin-screw extrusion would enhance the efficiency of CGTase-mediated starch modification, thereby producing potato starch with improved functional properties and resistance to digestive enzymes. By comparing different modification strategies, the goal is to provide scientific evidence and technical support for the functional enhancement and industrial applications (such as encapsulation, stabilizer, binding agent, film-forming, and gelling agent) of potato starch.

2. Materials and methods

2.1. Materials

Potato starch (No. S11004, amylose content 18.65 %, Biochemical Reagent grade) was purchased from Yuanye Bio-Technology Co., Ltd. (Shanghai, China). The moisture content of the starch was 17.76 %, determined by drying in a 105 °C oven (DHG-9240 A, Shanghai Jinghong Experimental Equipment Co., Ltd., Shanghai, China) for 4–6 h until starch reached a constant weight (Daudt et al., 2014). Referring to our previous study, the amylose content was measured using a spectrophotometric method (Zuo et al., 2024). Cyclodextrin glycosyltransferase (EC 2.4.1.19, declared activity: 3.0 KNU/g) from *Thermoanaerobacter* sp. (Toruzyme 3.0 L) was supplied by Novozymes Co., Ltd. (Shanghai, China). Pullulanase (EC 3.2.1.41, No. E-PULBL, 700 U/mL) from *Bacillus licheniformis* and glucose oxidase-peroxidase (GOPOD) assay kit were supplied by Megazyme International Ireland Ltd. (Wicklow, Ireland). α-Amylase (EC 3.2.1.1, No. 10080, 50 U/mg) from porcine pancreas and amyloglucosidase (EC 3.2.1.3, No. 10115, 70 U/mg) from *Aspergillus niger* were purchased from Sigma-Aldrich Chemical Co. (St. Louis, MO, USA). All other chemicals used were of analytical grade.

2.2. Preparation of PAW

In this study, PAW was generated by activating distilled water (DW) with a dielectric barrier discharge plasma system (CTP-2000KP, Nanjing Suman Electronics Co., Ltd., China). The distance between the plasma source and water was set to 4 mm. The quartz reaction chamber contained 60 mL of DW. The voltage regulator knob was adjusted to set the input power to 50 ± 1 W, with a discharge frequency of 10 kHz. The activation time was set to 10 min.

The temperature of PAW was measured using a temperature sensor (UT320D, UNI-T Co., Ltd., Guangdong, China). The pH and ORP of the prepared PAW were measured with a pH/ORP meter (FE20, Mettler-Toledo Instruments Co., Ltd., Shanghai, China), and the EC was measured using a conductivity meter (Leici DDS-307 A, Shanghai, China). PAW was used for analysis and experimentation immediately after preparation.

2.3. Treatment of starches

2.3.1. Extrusion of potato starch

Potato starch was extruded using a twin-screw extruder (TwinLab-F 20/40, Brabender, Oberhausen, Germany) with a round die at the extruder barrel outlet, with a length-to-diameter ratio of 40:1 and a die diameter of 5 mm. The extruder was equipped with a modular screw configuration featuring conveying elements and kneading blocks. The starch was fed into the extruder at a constant rate of 56 g/min. The in-barrel moisture content was maintained at 22 %. During extrusion, the temperature in the five controlled zones was set to 50, 70, 90, 90, and 70 °C, respectively (Zhou et al., 2022). The specific mechanical energy was approximately 168 kJ/kg. The samples were immediately freeze-dried using a freeze dryer (LGJ-10E, Sihuan Scientific Instrument Factory, Beijing, China), then the modified starch was ground, sieved, packaged, and stored for further study. NPS and ETN represent native starch and twin-screw extruded starch, respectively.

2.3.2. PAW treatment

NPS and ETN were directly mixed with PAW at room temperature (25 °C) and stirred (800 rpm) continuously for 10 min at a 1:2 (*w/v*) ratio using a magnetic stirrer (Heidolph MR Hei-Standard, Schwabach, Germany). The samples of NPS and ETN mixed with PAW were labeled as NPPA and ETPA, respectively. The samples were immediately freeze-dried, ground, sieved through a 150-μm screen, and stored fully sealed at 4 °C for further analysis.

2.3.3. Enzymatic modification of starch by CGTase

Following the method of Román et al. (2016), CGTase (0.2 U of CGTase/g of starch) was dissolved in 40 mL of phosphate buffer (20 mM, pH = 6.0) to prepare the enzyme solution. Then, pre-weighed NPS and ETN starch (10 g each) were suspended separately in 40 mL of the enzyme solution, with a solid-to-liquid ratio of 1:4 (*w/v*). The starch suspensions were thoroughly mixed with a glass rod, covered with plastic film to prevent drying, and incubated at 60 °C for 1 h. During incubation, the starch suspensions were thoroughly stirred every 15 min to prevent sedimentation of starch granules. The paste was then heated to 100 °C and maintained for 60 min. Afterward, the samples were immediately freeze-dried, ground into powder, and sieved through a 150-μm screen. The powder was stored fully sealed at 4 °C for further analysis. The NPS and ETN samples treated with CGTase were labeled NPCG and ETCG, respectively.

2.3.4. Multiple modification

The NPS and ETN starches were transferred to a beaker and sequentially modified with PAW and CGTase according to the conditions

described in Sections 2.3.2 and 2.3.3. The samples were labeled as NACG and EACG, respectively, and the freeze-dried samples were stored for further analysis. All starch treatments were carried out sequentially. The sequential application of these treatments enabled the individual effects of each modification to be studied.

2.4. Molecular structure

2.4.1. Chain length distribution (CLD)

The CLD of native and modified starch samples was determined according to the method of Su et al. (2020). Starch samples (40 mg) were dissolved in 2 mL of sodium acetate buffer (0.01 mol/L, pH 4.5) and heated in a boiling water bath for 20 min. After cooling, 7 μL of pullulanase (700 U/mL) was added, and the mixture was incubated for 24 h. The reaction was terminated by boiling for 20 min, followed by centrifugation at 4000 ×*g* for 10 min, and filtration through a 0.22 μm membrane. The filtrate was analyzed using high-performance anion-exchange chromatography coupled with pulsed amperometric detection (HPAEC-PAD, ICS-5000+, Thermo Fisher Scientific, USA) with a Dionex CarboPac™ PA-100 column. The mobile phases were 0.15 mol/L NaOH (eluent A) and 0.15 mol/L NaOH with 0.5 mol/L sodium acetate (eluent B) at a flow rate of 1 mL/min and a column temperature of 25 °C.

2.4.2. Molecular weight (M_w)

The molecular structure of native and modified starches was characterized using high-performance size-exclusion chromatography coupled with multi-angle laser light scattering and refractive index detection (HPSEC-MALLS-RI). A 60 mg sample was dispersed in 10 mL of 90 % (*v*/v) dimethyl sulfoxide solution to achieve a final concentration of 0.5 % (*w*/*v*). The mixture was heated in a boiling water bath for 1 h to ensure complete dissolution, followed by shaking at 30 °C and 180 rpm for 48 h. Subsequently, 9 volumes of absolute ethanol were added to the solution, and the mixture was centrifuged at 8000 rpm and 4 °C for 10 min. The precipitate was collected and washed twice with absolute ethanol. Prior to analysis, residual ethanol was evaporated, and the sample was redissolved in the mobile phase, then filtered through a 0.45 μm membrane filter (Maisinuo, Nanjing, China).

The solution was injected into an HPSEC system equipped with a multi-angle laser light scattering detector and a refractive index (RI) detector (Wyatt Technologies, Santa Barbara, CA, USA). Two columns were used in series: Shodex OHpak SB-806 HQ and SB-804 HQ (Showa Denko K.K., Kawasaki, Japan). The mobile phase consisted of 0.1 M $NaNO_3$, delivered at a flow rate of 0.6 mL/min. The column temperature was maintained at 50 °C. Data analysis was performed using Astra software (Version 5.3.4, Wyatt Technologies) (Kurdziel et al., 2022).

2.4.3. X-ray diffraction (XRD)

The crystal structure of native and modified starches was determined using an X-ray diffractometer (XD-3, Purkinje General Instrument Co., Ltd., China) with Ni-filtered CuKα radiation at 36 kV and 20 mA. The scanning range was set from 5° to 40° at a rate of 2°/min (Bragg & Bragg, 1913; Zuo et al., 2024). The relative crystallinity (RC) was calculated by the following equation:

$$RC = \frac{A_{crystalline}}{A_{crystalline} + A_{amorphous}} \quad (1)$$

where $A_{crystalline}$ represents the area of the crystalline peaks in the XRD pattern, and $A_{amorphous}$ represents the area of the amorphous scattering.

2.5. CDs content of starch samples

The composition of CDs from native and modified starches was analyzed using high-performance liquid chromatography (HPLC) (Ji et al., 2021). A 200 mg sample was dissolved in 5 mL ultrapure water, centrifuged, and the supernatant was injected (20 μL) into a Waters e2695 HPLC system with a 2414 RI detector (Waters, Inc., Torrance, CA, USA). An X-Bridge BEH Amide column (250 mm × 4.6 mm, Waters) was used. The mobile phase was 65 % by volume acetonitrile solution at 0.8 mL/min and 30 °C. Quantitative analysis was performed using the external standard method with known concentrations of α-CD, β-CD, and γ-CD standards. The concentration of each cyclodextrin was determined by correlating the peak areas with the standard curves, and the total CD content was calculated as the sum of α-CD, β-CD, and γ-CD.

2.6. Granule morphology

2.6.1. Scanning electron microscopy (SEM)

The microstructure of native and modified starches was observed using a scanning electron microscope (SU3500, Hitachi Co., Tokyo, Japan). Samples were examined under vacuum mode with a voltage of 10 kV. The starch samples were dispersed onto the sample stage and sputter-coated with gold prior to observation (Knoll & Ruska, 1932).

2.6.2. Confocal laser scanning microscopy (CLSM)

Each group of starch samples (10 mg) were mixed with 15 μL of 10 mmol/L APTS and 15 μL of 1 mol/L sodium cyanoborohydride, then stabilized at room temperature for 20 h. The stained starch samples were washed five times with 1 mL of DW and suspended in 100 μL of a 50 % glycerol-water mixture. A drop of this suspension was placed on a confocal laser scanning microscope (LSM900, Carl Zeiss AG, Germany) to observe the microstructure of the starch (Zuo et al., 2024).

2.6.3. Polarized light microscopy (PLM)

Native and modified starches were mixed with a glycerol solution (glycerol/H_2O, 1:1, *v*/v) to prepare a 1 % starch emulsion. A drop of the starch emulsion was placed on a glass slide to observe the structural properties of starch granules under a polarizing microscope (DM2700P, Leica, Germany) (Su et al., 2020).

2.7. Thermal properties

2.7.1. Starch gelatinization

The gelatinization behavior of native and modified starches was measured using a differential scanning calorimeter (DSC214, Netzsch, Germany). Potato starch was placed into an aluminum pan, and DW was added to achieve a starch-to-water ratio of 1:3. The pan was sealed and equilibrated overnight. Before testing, the sample pan was equilibrated at 20 °C for 3 min, then heated from 20 °C to 120 °C at a rate of 10 °C/min (Akhila et al., 2024; Watson et al., 1964).

2.7.2. Thermogravimetric analysis (TGA)

Native and modified starch samples (8.00 ± 0.02 mg) were weighed and placed on a platinum sample holder. TGA was conducted using a thermogravimetric analyzer (TGA5500, TA Instruments, USA), with a constant heating rate of 10 °C/min from 30 °C to 600 °C. High-purity helium gas (99.999 %, Air Products, USA) was used as carrier gas, with a 25 mL/min flow rate (Wei et al., 2024).

2.8. Low-field nuclear magnetic resonance

The water distribution of native and modified starches was determined using a low-field pulsed nuclear magnetic resonance analyzer (NMI20-025 V-I analyzer, Suzhou Niumag Analytical Instrument Corporation, China). Starch samples (0.05 g) were tightly packed to prevent water loss and placed in the magnet chamber. The T_2 spectra were obtained using the Carr-Purcell-Meiboom-Gill pulse sequence. The parameters for the measurements were set as follows: sampling point = 200,050, spectrum width = 200 kHz, waiting time = 1500 ms, time echo = 0.5 ms, number of echoes = 2000, and number of scans = 8 (Bloch, 1946; Zhong et al., 2024).

2.9. Solubility

The solubility of native and modified starches was determined over a temperature range of 50–90 °C. 0.5 g of starch was weighed into a 50 mL centrifuge tube and mixed with 25 mL of DW to prepare a 2 % (*w/v*) starch suspension. The suspension was thoroughly mixed and incubated in a shaking water bath at 50, 60, 70, 80, and 90 °C for 30 min. After incubation, the samples were cooled to room temperature and centrifuged at 4000 rpm for 10 min. The supernatant was collected and dried at 105 °C to a constant weight (Leach et al., 1959). The solubility was calculated using the following equation:

$$Solubility\,(\%) = \frac{W_1\,(Mass\ of\ supernatant\ in\ an\ aluminum\ box\ after\ drying)}{W\,(Starch\ sample\ weight)} \times 100\% \quad (2)$$

2.10. Rheological properties

The rheological properties of native and modified starches were measured using a rheometer (TA ARES G2, TA Instruments, USA) equipped with parallel non-deformable steel plates. The starch was dispersed in DW (10 % *w*/w). The sample was loaded onto the Peltier plate, and a thin layer of silicone oil was applied to prevent evaporation. Before measurement, the sample was equilibrated at 25 °C for 1 min. Following the method of Singh et al. (2008), gelatinization was conducted on the rheometer plate: the sample was first heated at 10 °C/min to 90 °C, held at 90 °C for 3 min, and then cooled to 25 °C, where it was equilibrated for 1 min. The linear viscoelastic region (LVR) was determined by strain sweep testing.

2.10.1. Small-amplitude oscillatory shear test

Frequency sweep tests were performed over a range of 0.1–100 rad/s with a strain amplitude of 0.2 %. The storage modulus (G′), associated with the gel's elastic properties, and the loss modulus (G″), reflecting its viscous properties, were obtained from the test results. The data were fitted using power law eqs. (3) and (4) to determine the frequency dependence of the gel samples and to analyze the effect of modification on the gel's characteristics (An et al., 2023).

$$G' = K' \cdot \omega^{n'} \quad (3)$$

$$G'' = K'' \cdot \omega^{n''} \quad (4)$$

where K' and K'' are modulus constants, n' and n'' are frequency exponents, and ω is the angular frequency.

2.10.2. Large-amplitude oscillatory shear (LAOS) test

The LAOS experiment was conducted with a strain sweep range of 0.01 % to 1000 % at a frequency of 1 Hz. Original waveforms under different strains were collected, and raw data on strain and stress were recorded. The Lissajous curves were obtained using the MITlaos program (MITlaos beta), representing the relationship between the raw stress response and strain over the entire oscillation cycle. These curves effectively describe nonlinear behavior and provide information on the contributions of elastic and viscous stresses to the total stress (Wei et al., 2024).

2.11. In vitro digestion

The contents of RDS, SDS, and RS in native and treated potato starches were determined according to the method described by Englyst et al. (1992). The intestinal simulation solution was prepared with deionized water containing porcine pancreatic α-Amylase (150 U/mL) and amyloglucosidase (80 U/mL). A 200 mg sample was suspended in 15 mL of 0.2 mol/L sodium acetate buffer, pre-equilibrated at 37 °C for 5 min, then mixed with 5 mL of the simulation solution for enzymatic hydrolysis in a constant-temperature water bath at 37 °C with agitation at 200 rpm. Aliquots (200 μL) of hydrolysate were collected at 0 min, 20 min, and 120 min intervals and immediately mixed with nine volumes of anhydrous ethanol to terminate the enzymatic activity. The resulting mixtures were subjected to centrifugation at 10,000 ×*g* for 5 min. The amount of glucose released in the supernatant was measured using a GOPOD assay kit. Starch content within 20 min, between 20 and 120 min, and after 120 min of digestion was defined as RDS, SDS, and RS, respectively.

2.12. Molecular docking

2.12.1. Docking of CGTase with starch molecules was performed

The conformations of CGTase (receptor) used in this study were obtained from the RCSB Protein Data Bank (ID: 1CYG) (https://www.rcsb.org/). Initially, Discovery Studio 2019 was used to remove water molecules and irrelevant heteroatoms, retaining only the protein structure. The 2D structure of linear amylose (ligand) was drawn using ChemDraw 20.0 (with four units), and the 3D structure of linear amylose was constructed using ChemDraw 3D. The MM2 algorithm (Casewit et al., 1992) was applied to optimize the conformation. Molecular docking simulations were performed using the libDock module in Discovery Studio 2019, and 3D visualization and analysis were conducted using PyMol 2.41 (https://pymol.org).

2.12.2. Docking of α-CD, β-CD, and γ-CD with amylopectin and amylose

The crystal structures of α-CD, β-CD, and γ-CD were extracted from the RCSB Protein Data Bank with the IDs 2ZYM, 3CGT, and 2ZYK, respectively (Gannimani et al., 2015). The models were then imported into Autodock Tools (ADT, Version 1.5.7) for hydrogenation and charge adjustment. Molecular docking of CDs (receptors) and starch (ligands) was performed using Autodock Vina software (Trott & Olson, 2010). The active site was set to cover the regions of amylopectin and amylose as the docking box, and the optimal conformation was selected for binding mode analysis. Visualization of the binding site and hydrogen bonds was conducted using PyMol 2.41.

2.13. Statistical analysis

All experiments were performed at least in triplicate, with results presented as mean ± standard deviation. The data were analyzed using SPSS 22.0 software (SPSS Inc., Chicago, USA). One-way analysis of variance (ANOVA) was used to compare the relationships between variables, and Duncan's multiple range test was applied to determine whether there were significant differences between the means ($p < 0.05$).

3. Results and discussion

3.1. Physicochemical characterization of plasma-activated water

Table S1 presents the physicochemical properties of distilled water after CP treatment. CP treatment significantly altered ($p < 0.05$) the physicochemical properties of the water. The CP treatment reduced the pH of DW from 6.58 to 3.21, as CP facilitated the dissolution of nitrogen oxides formed from N_2 and O_2, leading to water acidification (Akhila et al., 2024). EC reflects the concentration of reactive ions in water, and ORP indicates the redox potential of the water (Zou, Tan, et al., 2024). CP treatment increased the water's EC from 3.41 μS/cm to 325.72 μS/cm and raised the ORP from 265 mV to 587.33 mV. This behavior could be attributed to the increased presence of reactive ions and oxidizing substances (Zou et al., 2025). No significant difference in DW temperature was observed before and after activation, suggesting that CP treatment had a minimal effect on water temperature.

3.2. Molecular structure characterization

3.2.1. Chain length distribution

Based on the periodic distribution pattern of amylopectin chain length proportions, the range was divided into five sections: DP < 6, DP 6–12, DP 13–24, DP 25–36, and DP > 36 (Ji et al., 2020). The proportion of different chain lengths in starch reflects its intrinsic fine structure and is closely related to its properties, such as gelatinization and digestion characteristics (Benavent-Gil et al., 2021). The chain length distribution of starch is shown in Fig. 1 and Table S2. NPS showed a typically high proportion of DP 13–24 chains (64.85 %), reflecting its relatively long branched structure, which favors the formation of well-ordered double-helical structures and crystalline regions. Starch treated with extrusion showed no significant differences from NPS (except for DP > 37). This could be due to the large molecular chains of amylopectin, where shear-induced breakage results in relatively fewer and smaller fragments (Sun et al., 2021). The PAW-induced starch branch depolymerization through reactive free radical action, leading to an increase in the short-chain fraction. This was because the free radicals broke longer branches, which is consistent with the findings reported by Sun et al. (2021). The increase in short chains promoted the formation of double-helix structures, thereby enhancing the crystallinity of starch.

The EACG treatment had the most significant effect on the fine structure of starch, with long chains (e.g., DP > 37) almost completely degraded, resulting in a large increase in short-chain starch (DP < 6 accounted for 73.13 %). This indicates that extrusion and PAW treatments effectively facilitated starch hydrolysis by CGTase (Li et al., 2021). Extrusion treatment disrupted the crystalline structure of starch through mechanical forces, improving molecular accessibility to CGTase and generating shorter chains. The depolymerization of amylopectin branches induced by PAW's reactive free radicals was greater than the degree of polymerization (Sun et al., 2021), also enhancing the efficiency of enzyme-mediated short-chain production, consistent with previously reported findings on changes in the fine structure of potato starch (Li et al., 2021).

3.2.2. Molecular weight distribution analysis

The molecular structure of starch has a significant influence on its properties, with molecular weight distribution being a key structural characteristic. As shown in Table S2, compared to native starch, both PAW and extrusion treatment reduced the M_w of starch. The ROS in PAW attacks starch molecular chains, causing glycosidic bond cleavage and subsequent chain shortening. Extrusion processing, which involves high temperature, high pressure, and intense shear forces, disrupts the granular structure of starch and breaks long chains into shorter ones (Sun et al., 2021). Modification catalyzed by CGTase demonstrated the most efficient regulation of M_w, with M_w significantly reduced by 71.93 % ($p < 0.05$). This is attributed to the specific hydrolysis of glycosidic bonds and the chain-shortening effect associated with cyclodextrin formation (Ji et al., 2021). The number-average molecular weight (M_n) is the statistical average molecular weight of polymer chains in the sample. Extrusion treatment increased the M_n value through cross-linking and partial gelatinization, while PAW and CGTase treatments decreased the M_n value through free radical action, oxidation, and enzymatic hydrolysis (Ji et al., 2021; Kurdziel et al., 2022).

The polydispersity index (PDI) of starch molecules can also effectively reflect the distribution characteristics of the starch molecular weight. The PDI of the modified starches was significantly reduced ($p < 0.05$), indicating a more uniform molecular chain length distribution. This is consistent with an increased proportion of short chains and a decrease in long chains within the CLD. The narrowing of molecular weight distribution and enhanced structural regularity may improve the functional performance of starch by modulating digestion rate (making it more easily encapsulated by CDs), thereby enhancing its application potential in low-glycemic index (GI) food additives or drug sustained-release carriers. These results provide a theoretical basis for the precise design of functional starch materials (Ab'lah et al., 2023).

3.2.3. Crystal structure

According to the XRD patterns (Fig. 2A and Table S2), potato starch exhibits a B-type crystalline structure, with main peaks at angle 2θ values of 17.2° and a double peak at 22–24°. The RC values of all starches ranged from 21.45 % to 23.89 %. Compared to native starch, the RC of the ETN group was significantly reduced by 2.3 % ($p < 0.05$), whereas the PAW-treated group showed a significant increase of 8.8 % ($p < 0.05$). Extrusion is a mechanical disruption process that directly damages starch granules and molecular arrangement through high pressure and shear, transforming the original B-type crystalline structure into an amorphous structure (Akhila et al., 2024). PAW treatment may induce starch molecule rearrangement by generating ROS. This effect may enable some amorphous regions to regain a degree of crystallinity, thereby increasing the starch's crystallinity (Yan et al., 2024).

The RC values of CGTase hydrolyzed starch (NPCG group) decreased to zero, and a relatively broad amorphous peak appeared at 20.5° in the XRD spectra of potato starch in the ETCG and EACG groups. This was due to extrusion disrupting the B-type crystalline structure of the starch, breaking hydrogen bonds within the potato starch granules, and enabling water to bind to free hydroxyl groups. Subsequent CGTase hydrolysis rendered the starch amorphous, eliminating its crystalline characteristics (Liu et al., 2009).

3.3. Water distribution

The water distribution in starch is closely related to its properties, including gelatinization, gelation, retrogradation, and structural characteristics (Zhuang et al., 2023), Fig. 2B shows the transverse relaxation (T_2) spectrum of starch, corresponding to three peaks (T_{21}, T_{22}, and T_{23}). Shorter relaxation times indicate more restricted water mobility due to substrate binding. Accordingly, T_{21} (0.1–10 ms) represents bound water, T_{22} (10–100 ms) represents weakly bound water, and T_{23} (100–10,000 ms) represents free water (Zhuang et al., 2023).

The T_{21} peak of extruded starch was higher than that of native starch, while the T_{23} peak was lower, a similar phenomenon observed in the PAW group. This indicates a water transition from a free to a bound state, likely due to the breakage of starch molecular chains during extrusion, which exposed many hydrophilic hydroxyl groups (Zeng et al., 2022). PAW may alter the hydrogen-bonding structure or molecular polarity of water, enhancing hydrogen bonding between water molecules and starch chains, thus promoting the formation of bound water (Sun et al., 2021). The ETPA group showed the highest T_{21} peak and the lowest T_{23} peak under the synergistic effects of PAW and extrusion. The increase in bound water enhances starch adhesion and texture stability in food, which in turn improves food texture and mouthfeel. This is beneficial for applications in fields such as baking and frozen foods (Wang & Copeland, 2013). The NMR T_2 spectrum of CGTase-treated potato starch shows a decrease in bound water and an increase in free water. The CDs formed after CGTase treatment may reduce direct contact between water and starch structure through encapsulation, causing water to more readily exist as free water (Benavent-Gil et al., 2021).

3.4. Composition analysis of CDs in modified starches

To investigate the effects of CGTase, extrusion, and PAW on starch modification, the composition of CDs in the modified products was analyzed. As shown in Fig. 2C, the CDs yield from starch pretreated with extrusion and PAW was significantly higher ($p < 0.05$) than that of the NPCG group. Extrusion disrupts the crystalline structure of starch, making the starch molecules more amorphous through high temperature, pressure, and shear, thereby increasing enzyme binding sites and facilitating CGTase attack on the starch chains. This enhances the yield of α-, β-, and γ-CDs (Román et al., 2016; Yan et al., 2024). PAW can alter

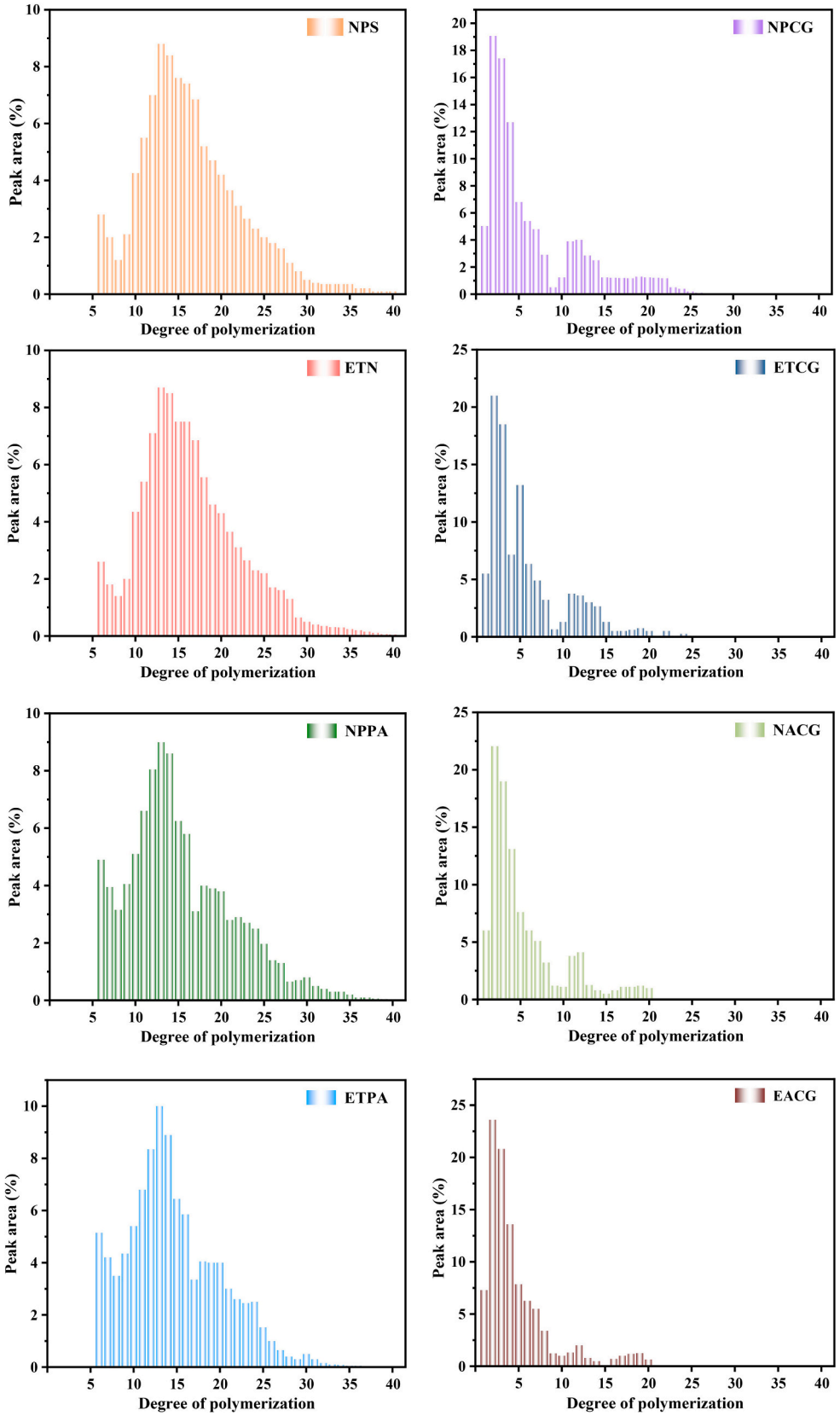

Fig. 1. Chain length distribution analysis of potato starches. NPS: Native starch; ETN: Twin-screw extruded starch; NPPA: NPS mixed with PAW; ETPA: ETN mixed with PAW; NPCG: NPS treated with CGTase; ETCG: ETN treated with CGTase; NACG: NPS sequentially treated with PAW and CGTase; EACG: ETN sequentially treated with PAW and CGTase.

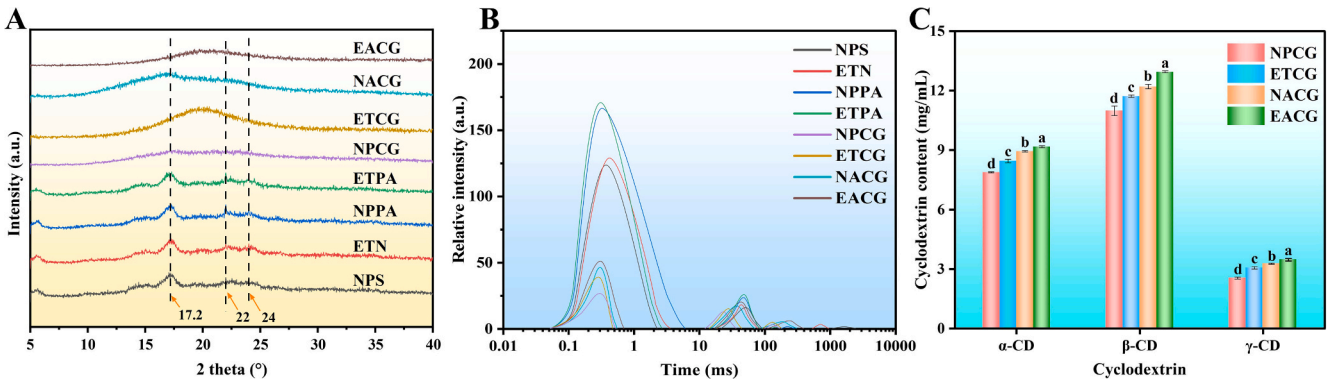

Fig. 2. XRD spectra (A), T2 relaxation time distribution (B), and cyclodextrins content (C) of potato starches. NPS: Native starch; ETN: Twin-screw extruded starch; NPPA: NPS mixed with PAW; ETPA: ETN mixed with PAW; NPCG: NPS treated with CGTase; ETCG: ETN treated with CGTase; NACG: NPS sequentially treated with PAW and CGTase; EACG: ETN sequentially treated with PAW and CGTase.

the physicochemical properties of starch, increase its surface activity and solubility, making it easier for CGTase to act on the starch molecules and thereby promoting the production of α-, β-, and γ-CDs (Sun et al., 2021). Among all groups, the EACG group had the highest CDs yield, attributed to the synergistic effect of extrusion and PAW.

3.5. Granule morphological structure

As shown in Fig. 3, A1-A8 were SEM images of potato starch. The surface of NPS granules was smooth, with a circular or oval shape of varying sizes. However, after treatment with PAW and extrusion, the starch surface became rough, eroded, and damaged. PAW treatment caused damage due to the etching action of PAW, where ROS in PAW reacted with molecules on the starch surface, leading to structural erosion (Zuo et al., 2024). The starch in the ETN group exhibited greater damage, with granules becoming irregular in shape. This could be attributed to the exposure of starch granules to high temperatures, shear forces, pressure, and rapid moisture changes during the extrusion process (Ali et al., 2020). Due to the synergistic effects of PAW and extrusion, the ETPA group starch exhibited more severe granule structure disruption than single modifications. The granules appeared as irregular blocks with noticeable pits and cracks. In the SEM images of CGTase-modified starch, irregular polyhedral or flaky shapes were observed. This semi-crystalline structure is related to intramolecular and

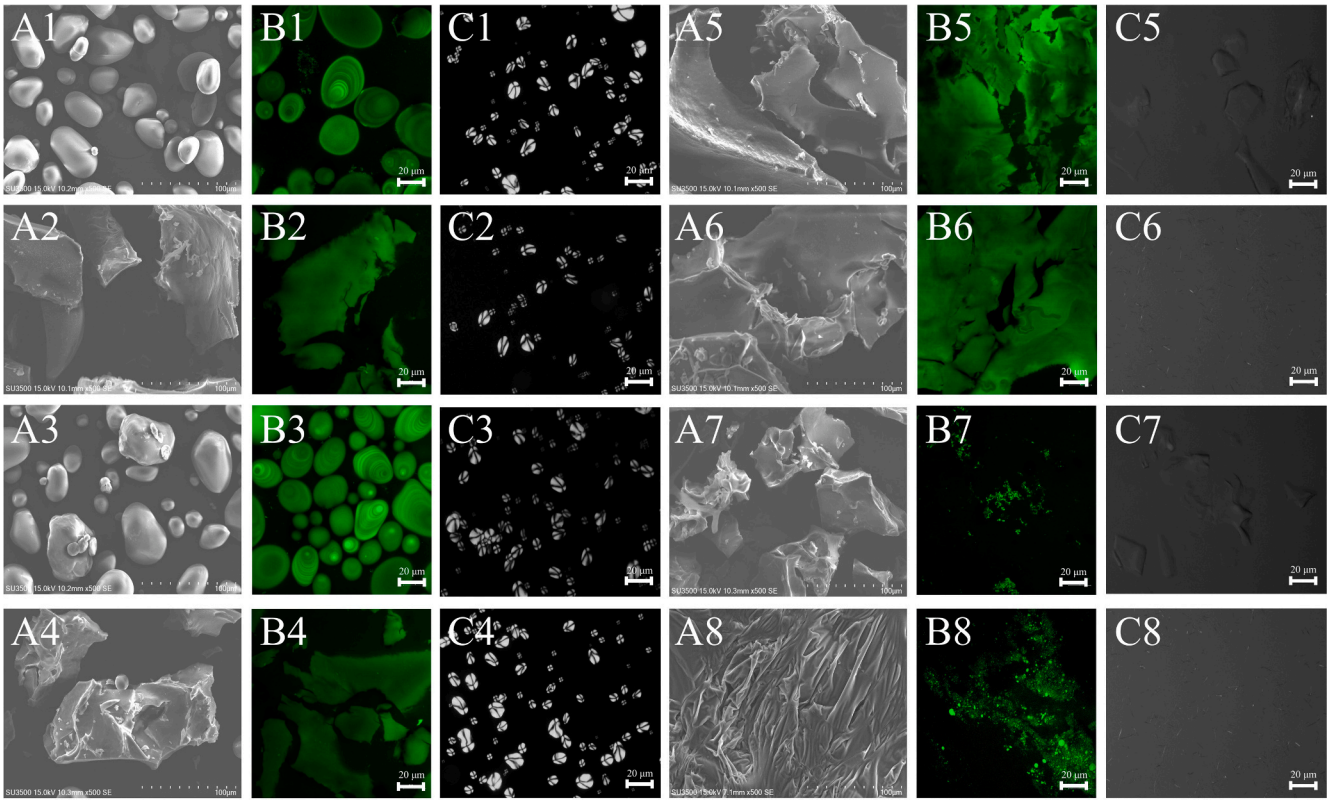

Fig. 3. Scanning electron micrographs (500×, A1-A8), confocal laser scanning micrographs (20 μm, B1-B8), and polarized light micrographs (20 μm, C1-C8) of native and modified potato starches. For A1, B1, C1, NPS; A2, B2, C2, ETN; A3, B3, C3, NPPA; A4, B4, C4, ETPA; A5, B5, C5, NPCG; A6, B6, C6, ETCG; A7, B7, C7, NACG; A8, B8, C8, EACG.
NPS: Native starch; ETN: Twin-screw extruded starch; NPPA: NPS mixed with PAW; ETPA: ETN mixed with PAW; NPCG: NPS treated with CGTase; ETCG: ETN treated with CGTase; NACG: NPS sequentially treated with PAW and CGTase; EACG: ETN sequentially treated with PAW and CGTase.

intermolecular hydrogen bonding between amylose and amylopectin chains (Aguado et al., 2021). In the EACG group, swollen starch granules were observed to adhere to one another, resulting in increased viscosity. This phenomenon may be due to the dual modification by PAW and CGTase under extrusion, which likely caused entanglement between amylose chains or between amylose and amylopectin side chains, forming an amylose gel network (Wu et al., 2022).

CLSM was used to further characterize microstructure and morphological changes, as shown in Fig. 3B1—B8. Native potato starch exhibited distinct growth rings and hilum. The growth rings displayed alternating light and dark regions, representing the alternating amorphous and crystalline zones. APTS was used to label the reducing ends of starch molecules. Since amylose contains more reducing ends, there is a positive correlation between amylose content and fluorescence intensity in starch observed by CLSM (Parker & Ring, 2001). The fluorescence intensity at the center of potato starch granules was higher than at the periphery, indicating that the hilum region contains more amylose. The PAW-treated starch showed distinct growth rings, suggesting that the etching effect of PAW occurred primarily on the starch surface, with minimal damage to the internal structure. In contrast, the growth rings and hilum structures of starch modified by extrusion and CGTase were disrupted. This disruption resulted from the breakdown of crystalline and amorphous regions caused by CGTase hydrolysis, high temperatures, and shear forces (Liang et al., 2024).

Fig. 3C1—C8 shows PLM images of starch. The high degree of order in the crystalline regions of starch gives these areas different refractive indices for light in various directions, resulting in birefringence and forming a Maltese cross (Xie et al., 2013). In the non-CGTase-treated groups, the Maltese cross of the starch granules was clearly observed, with their position and brightness being essentially unaffected by PAW and extrusion treatments. This indicates that PAW and extrusion treatment do not completely disrupt the order of all starch crystals, which is consistent with the results of Srangsomjit et al. (2022). After modification with CGTase, the Maltese cross of the starch disappeared, indicating

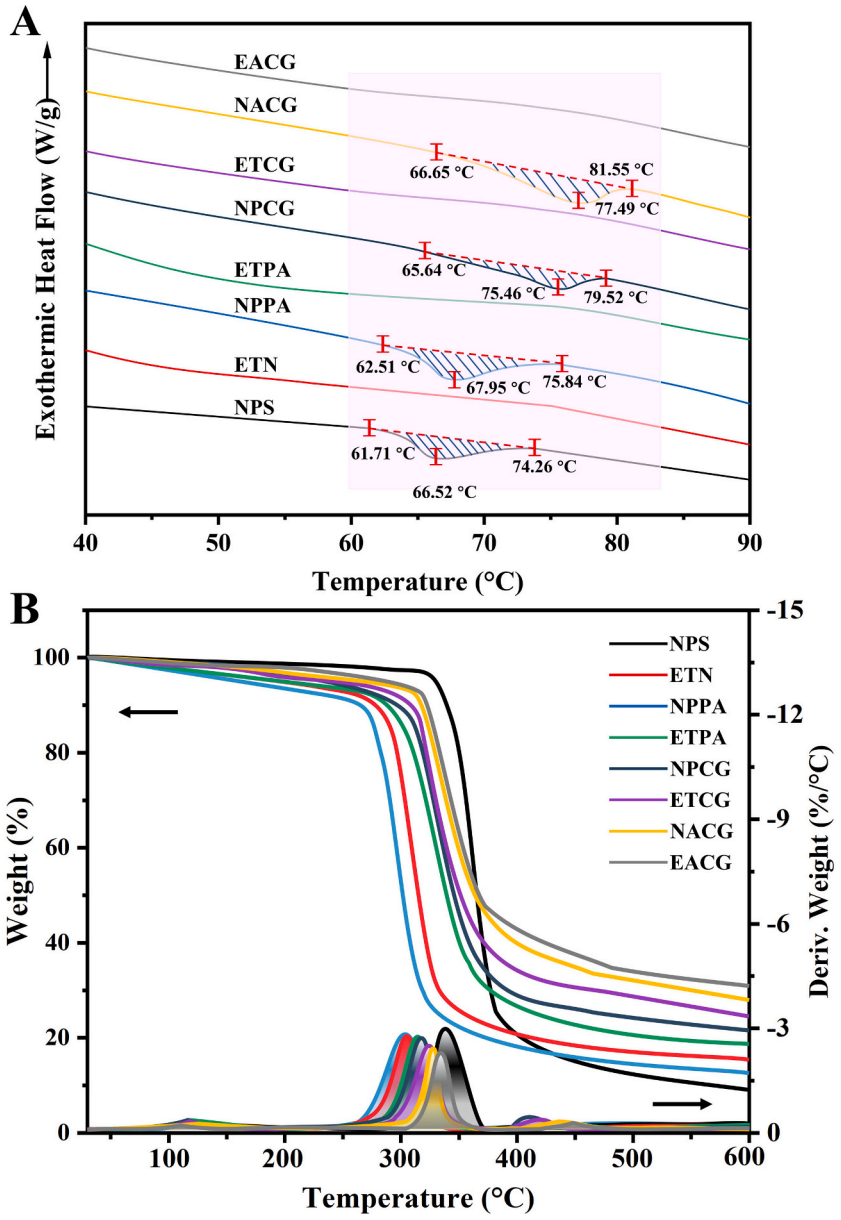

Fig. 4. DSC (A) and TG (B) thermograms of native and modified starches. NPS: Native starch; ETN: Twin-screw extruded starch; NPPA: NPS mixed with PAW; ETPA: ETN mixed with PAW; NPCG: NPS treated with CGTase; ETCG: ETN treated with CGTase; NACG: NPS sequentially treated with PAW and CGTase; EACG: ETN sequentially treated with PAW and CGTase.

that CGTase treatment severely disrupted the double-helix structure of amylopectin in the crystalline lamellae, reducing the molecular order (Wang et al., 2022). Bright needle-like particles were observed in the CGTase-treated group, indicating that CDs possess a certain degree of crystallinity. However, due to the dispersed state of CDs within the samples, XRD did not detect crystalline peaks in the CGTase-treated samples.

3.6. Thermal performance analysis

Fig. 4A and Table S3 show the thermal properties of the samples. Gelatinization temperature reflects the thermal stability of starch granules, while the ΔH is directly related to the retrogradation tendency of starch. Both NPS and PAW-treated starches exhibited endothermic peaks, while no peak was observed in the extrusion-treated starch, indicating that its double helix structure was severely disrupted. As the amorphous regions of the starch increased, there was no distinct melting point or phase transition during heating, resulting in the absence of a significant endothermic signal in DSC measurements. These findings align with the XRD and microstructural results. Compared to native starch, the gelatinization temperature and enthalpy (increased from 12.61 J/g to 15.66 J/g) of PAW-treated starch significantly increased ($p < 0.05$). The corn starch treated with PAW also showed a similar trend, with a decrease in gelatinization temperature and enthalpy after treatment (Zuo et al., 2024). This increase is likely due to the ROS in PAW enhancing the crystalline structure. The increase in T_c-T_o indicates a decrease in crystalline uniformity. For CGTase-modified starch, the endothermic peak and T_c-T_o shifted to higher temperatures, while ΔH significantly decreased ($p < 0.05$) compared to native starch. This may be due to the shortening of starch molecular chains after CGTase treatment, with shorter chains being more prone to molecular movement during thermal processing. The structural changes increase the energy required to disrupt the remaining starch structure, leading to a higher gelatinization temperature (Ji et al., 2020).

TG was used to further characterize the thermogravimetric properties of the samples (Fig. 4B). The thermal decomposition process of the samples exhibited three main regions. The first weight loss peak appeared in the range of 60 °C to 130 °C, mainly attributed to the vaporization of water in the starch samples, marking a physical weight loss process. The second thermogravimetric weight loss peak, occurring between 230 °C and 360 °C, was attributed to the degradation of starch. The third weight loss peak, observed in the range of 380 °C to 460 °C, was due to the decomposition of CDs (Wu et al., 2020). Extrusion, PAW, and CGTase significantly reduced the weight loss rate and velocity. This may be due to PAW and extrusion strengthening intermolecular interactions within the starch, thereby decreasing the weight loss rate and enhancing the starch's thermal stability (Wei et al., 2024). After CGTase treatment, part of the starch was converted into CDs. These cyclic molecular structures exhibit high stability due to the formation of an internal hydrogen-bond network, which enhances their resistance to thermal decomposition and slows the rate of weight loss (Ji et al., 2020).

3.7. Solubility

As shown in Table S3, the solubility of all samples increased significantly with rising temperature, indicating that higher temperatures promoted starch dissolution. This may be attributed to the enhanced migration of amylose from the crystalline regions of amylopectin, promoting leaching and solubilization (Ge et al., 2021). Compared with native starch, the solubility of extrusion, PAW, and CGTase-modified starches was significantly higher ($p < 0.05$). This improvement may result from the disruption of the ordered crystalline regions by high temperature and shear during extrusion, which increases the availability of water-binding sites, thereby enhancing solubility. The ROS in PAW can oxidize and cleave the starch chains, generating smaller and more soluble fragments (Zuo et al., 2024). Sun et al. (2021) reported that both cold plasma and twin-screw extrusion treatments can increase the solubility of potato starch, with the combined treatment of cold plasma and extrusion showing a more significant synergistic effect.

The CGTase-modified group exhibited significantly higher solubility compared to the individual physical modification groups (extrusion and PAW). CGTase specifically hydrolyzes starch chains and catalyzes the formation of CDs, generating short-chain cyclic products whose hydrophilic exterior structures enhance intermolecular hydration, thereby improving solubility (Li et al., 2014). In addition, the EACG group demonstrated the highest solubility (84.55 % at 90 °C), suggesting that the synergistic effect of extrusion/PAW and CGTase treatment may disrupt the crystalline regions of starch granules through mechanical shearing and oxidative actions. This process likely produces smaller soluble fragments and exposes more enzymatic binding sites, thus facilitating the efficient synthesis of CDs (Román et al., 2016).

3.8. Rheological properties analysis

3.8.1. Small-amplitude oscillatory shear test

The gel properties of NPS and modified potato starches are shown in Fig. 5A-B, indicating different frequency dependencies among the samples. For all starch gels, G′ is greater than G″, indicating elasticity-dominant characteristics, manifesting a solid-like or gel-like structure (Wei et al., 2024). The G′ and G″ values of all treated groups were higher than those of the control group, with the EACG group showing the highest G′ and G″ values. This indicates that PAW, extrusion, and CGTase treatments can enhance the viscoelasticity and mechanical properties of starch gels. This may be because PAW, by initiating oxidation reactions, increases intermolecular interactions within the starch. Extrusion treatment disrupts the crystalline structure of starch granules through high temperature and pressure, promoting gelatinization or hydrolysis and enhancing rheological properties (Sun et al., 2021), and CGTase, by catalyzing glycosyl transfer, alters the arrangement or crosslinking of starch molecular chains, forming a stronger molecular network (Benavent-Gil et al., 2021).

The frequency sweep results were fitted using a power law model, with the fitting results listed in Table S4. K′ and K″ reflect the gel's elasticity and viscosity, respectively. The increased K′ and K″ values for modified starches indicate stronger elastic networks and enhanced viscous properties. n' and n″ represent the frequency dependence of G′ and G″, respectively; smaller n values indicate lower frequency dependence of G (An et al., 2023). The n values for all samples were close to 0, indicating that all samples exhibited non-Newtonian fluid characteristics (Zhong et al., 2024).

3.8.2. Large-amplitude oscillatory shear (LAOS) test

As shown in Fig. 5C, LAOS was used to further evaluate the viscoelastic properties of the gels under complex strain amplitudes. Within the LVR, G′ was greater than G″ for all samples, indicating that strain or stress in this region did not cause disruption or reorganization of the gel network, with the gel exhibiting primarily elastic behavior. As strain amplitude increased, G′ declined rapidly, and G″, after a brief increase, also began to decrease. This represented type III nonlinear viscoelastic behavior (weak strain overshoot), typical of many soft glassy materials (An et al., 2023). At lower stress levels, the internal structure of the gel undergoes rearrangement due to shear stress, causing G″ to increase gradually. As stress continues to increase, the supporting structure of the gel network is disrupted, leading to a rapid decrease in G′, with shear energy being converted into the loss modulus. This results in the overshoot behavior of G″ (Wei et al., 2024).

In this study, the viscoelastic properties of starch gels were primarily attributed to the disruption and reorganization of the gel network (Fig. 5D). Region 0 shows the heating process of starch, during which starch molecular chains are released from within granules and dissolve in water. As the temperature decreases, these molecular chains rearrange through intermolecular interactions, such as hydrogen bonding, to

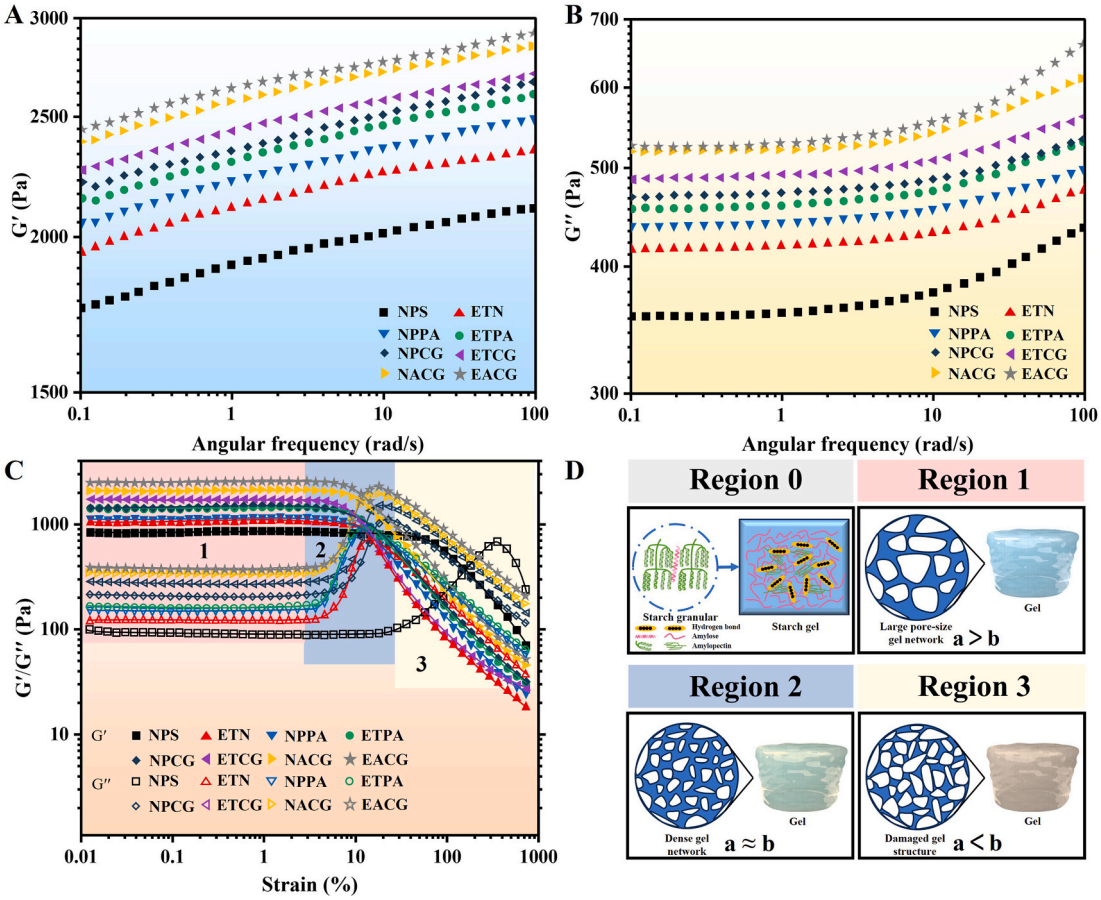

Fig. 5. Rheological property tests of different potato starch samples, storage modulus G′ (A), loss modulus G″ (B), and large amplitude oscillatory shear (C). Schematic diagram of structural changes in the gel under large amplitude oscillatory shear (D). NPS: Native starch; ETN: Twin-screw extruded starch; NPPA: NPS mixed with PAW; ETPA: ETN mixed with PAW; NPCG: NPS treated with CGTase; ETCG: ETN treated with CGTase; NACG: NPS sequentially treated with PAW and CGTase; EACG: ETN sequentially treated with PAW and CGTase.

form a three-dimensional network structure, ultimately resulting in a gel with certain elastic and viscous properties upon cooling (Zheng et al., 2024). In Region 1 of all treated sample groups, as the strain increased, the rate of network formation (a) exceeded the rate of disruption (b), meaning that the overall network structure increased. Molecules form a complex, large-pore network structure through intermolecular interactions (Fan et al., 2019). A local maximum in G″ appeared in Region 2, where the disruption and network formation rate were approximately balanced (a ≈ b). At this point, the gel network structure was most dense and porous (Hyun et al., 2011). However, as strain continued to increase, the disruption rate exceeded the formation rate (a < b), leading to irreversible structural damage, with both the G′ and G″ beginning to decline, displaying softening behavior (Region 3). The strain point at which the G′ and G″ of NPS began to decline lagged behind that of modified starch, with Regions 1, 2, and 3 also shifting relatively later. This may be due to the more stable molecular structure of native starch, with stronger intermolecular interactions and greater resistance to deformation (Yu et al., 2022).

3.8.3. *Lissajous curve analysis*

Lissajous plots can be used to visualize the relationship between total stress, elasticity, and viscosity of the samples as they transition from the linear to the nonlinear region (An et al., 2023). Fig. 6 shows the Lissajous plots of the samples. The red loop represents total stress, while the blue lines in Fig. 6A-B represent elastic and viscous stress, respectively. In the LVR in Fig. 6A, total stress is closer to the elastic component (blue line), indicating that the starch gel is primarily elastic. As amplitude gradually increases and the samples enter the nonlinear region, the narrow elliptical shape of the plot broadens, indicating that the gel system exhibits viscosity-dominated shear-thinning behavior (Wei et al., 2024).

In Fig. 6B, when strain is at a lower value, the total stress line of the Lissajous curve appears elliptical, indicating that the gel exhibits primarily elastic behavior. As the stress amplitude increases, the curve gradually narrows from a circular shape, suggesting that viscous stress progressively dominates the total stress. The elastic Lissajous loop area of the EACG group is the largest, indicating that more energy is required to complete the oscillatory shear of the sample. This suggests that the mechanical properties of the EACG-modified gel have been enhanced (Wei et al., 2024). This may be due to the introduction of CD structures through CGTase treatment, which promotes additional bridging interactions between molecular chains (Cheng et al., 2024).

3.9. *In vitro digestive analysis*

Fig. 7 shows the contents of RDS, SDS, and RS in starch. Native starch contained 36.15 % RDS, 32.16 % SDS, and 31.69 % RS. Extrusion, PAW, and CGTase treatments increased the SDS and RS contents while reducing the RDS content. This may be attributed to extrusion disrupting the weaker crystalline structures in starch, leaving the remaining crystalline structures more stable and less susceptible to rapid degradation by digestive enzymes. The reactive species in PAW increased the ordered structure of starch, making it more resistant to hydrolysis by digestive enzymes. This is consistent with the results of the XRD analysis.

The slow-digestion and resistant-digestion properties of CGTase-modified starch were significantly enhanced ($p < 0.05$), likely due to CDs having a certain resistance (Li et al., 2019). Additionally, the unique

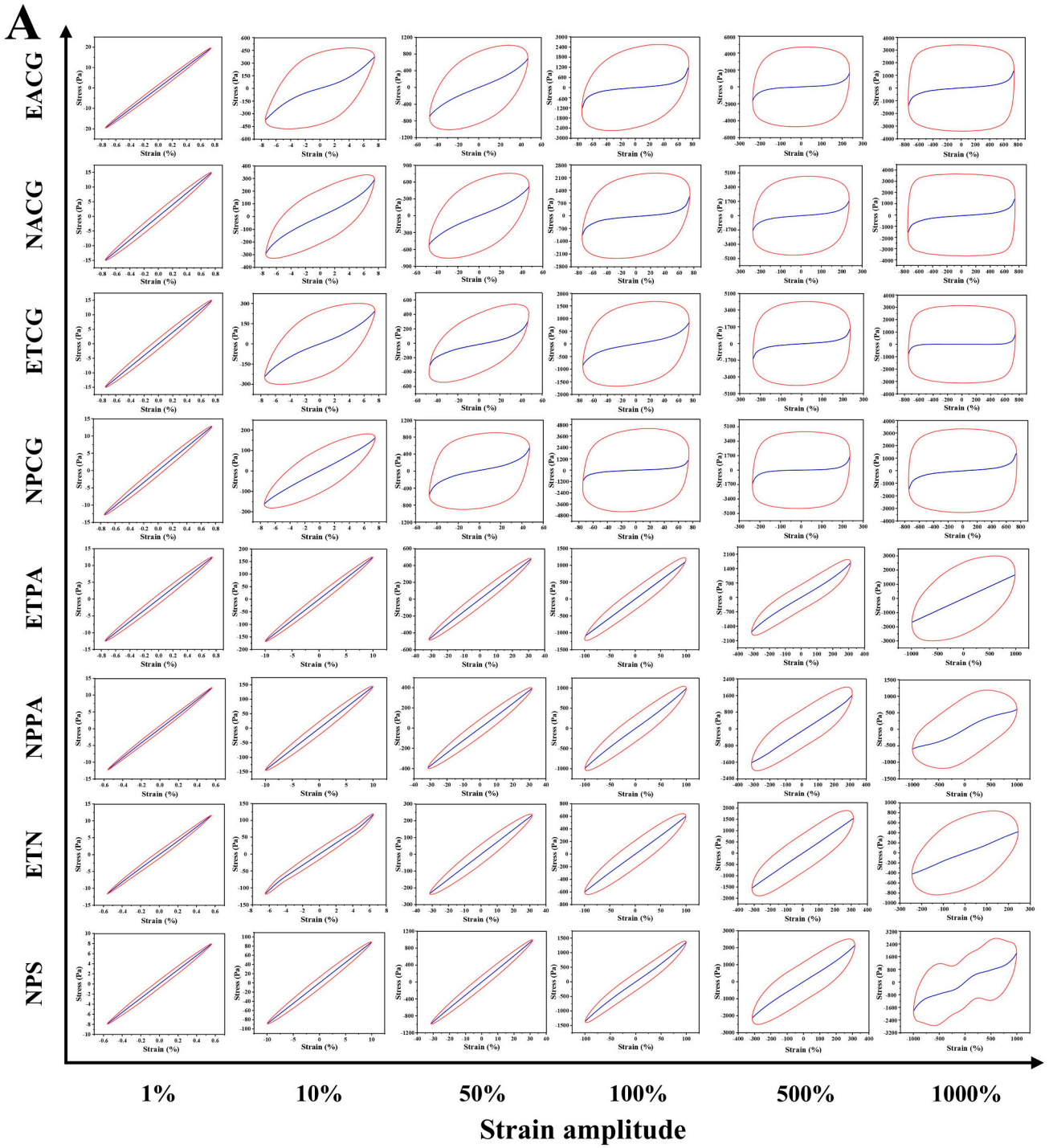

cyclic structure of CDs hydrophobically encapsulated the glucose residues of starch, making them more resistant to enzymatic hydrolysis. The molecular mechanism underlying this reaction will be further analyzed through molecular docking in Section 3.9. The resistant starch content of potato starch was significantly increased by EACG modification, rising from 31.69 % to 61.38 %. This was due to the combined effects of extrusion's mechanical force and PAW's oxidation, which created a structure more amenable to CGTase modification. Additionally, the long chains of amylopectin were degraded into shorter chains, which are more easily encapsulated by CDs. This will help in producing foods with lower glycemic index and higher resistant starch content.

3.10. Molecular docking analysis of CGTase and CDs with starch

3.10.1. Analysis of the docking mechanism between CGTase and starch

CGTase primarily acts on the α-1,4-glycosidic bonds of starch molecules, making amylose an ideal model to display CGTase's binding sites and catalytic mechanism (Ji et al., 2021). To investigate this, molecular

Fig. 6. Lissajous curves of different potato starch gels, elastic Lissajous curves (A) and viscous Lissajous curves (B). NPS: Native starch; ETN: Twin-screw extruded starch; NPPA: NPS mixed with PAW; ETPA: ETN mixed with PAW; NPCG: NPS treated with CGTase; ETCG: ETN treated with CGTase; NACG: NPS sequentially treated with PAW and CGTase; EACG: ETN sequentially treated with PAW and CGTase.

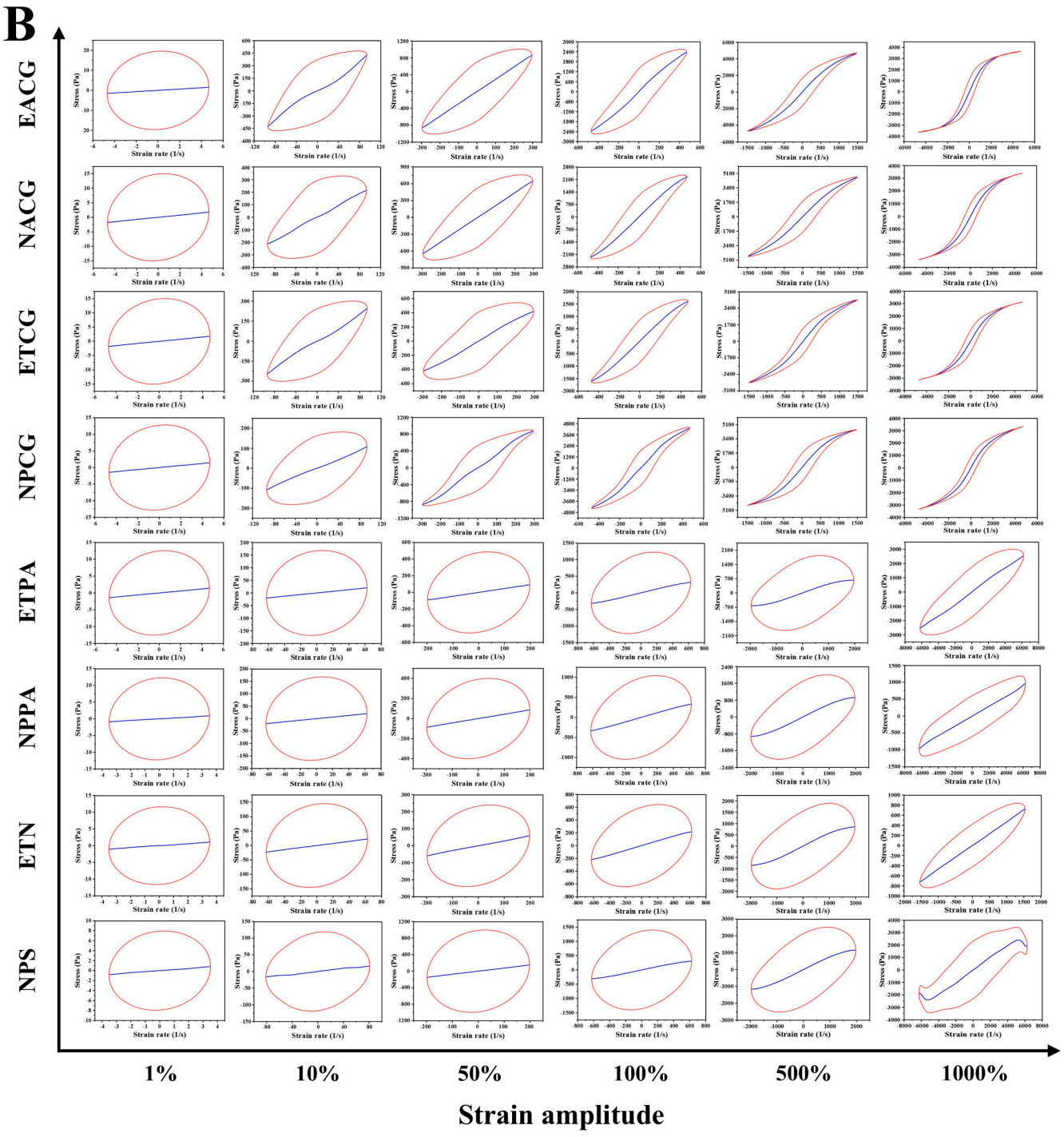

Fig. 6. (*continued*).

docking was used to study the specific binding relationship between amylose and CGTase (Fig. 8). Using the LibDock module, the highest-scoring ligand-receptor interaction yielded a LibDockScore of 166.454. Five amino acid residues (ASN270, ASP311, GLU573, GLY607, and GLU605) formed stable hydrogen bonds with starch residues, creating six hydrogen bond pairs within a spherical docking region of 10 Å, with bond lengths ranging from 1.8 to 2.74 Å. Additionally, TYR267, GLU271, and LYS613 formed weak carbon-hydrogen interactions with the glucose residues of amylose. These results indicate a stable interaction between amylose and CGTase, showing a high binding affinity (van der Veen et al., 2000).

ASN270, TYR267, GLU271, and ASP311 are in the A domain of CGTase, which is the primary catalytic region responsible for substrate binding and conversion. GLU573, GLU605, GLY607, and LYS613 are in the E domain, a unique CGTase feature containing two maltose-binding sites. These sites interact with glycosyl groups on the substrate through hydrogen bonding and hydrophobic interactions, aiding in the positioning and stabilization of amylose at the binding site (Lawson et al.,

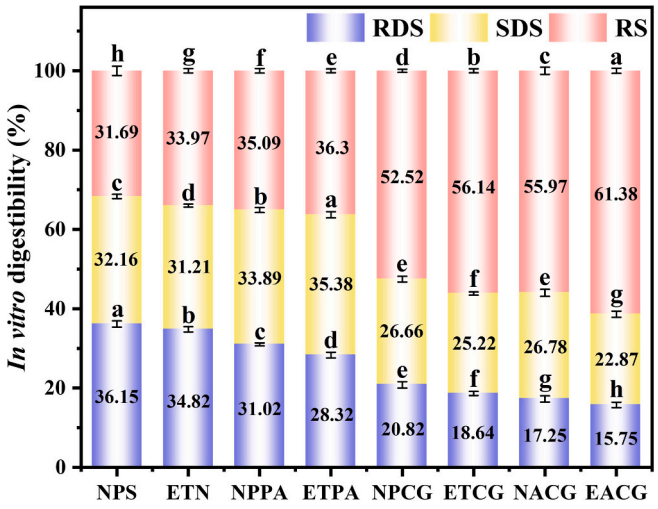

Fig. 7. Contents of RDS, SDS, and RS in native and modified starches. NPS: Native starch; ETN: Twin-screw extruded starch; NPPA: NPS mixed with PAW; ETPA: ETN mixed with PAW; NPCG: NPS treated with CGTase; ETCG: ETN treated with CGTase; NACG: NPS sequentially treated with PAW and CGTase; EACG: ETN sequentially treated with PAW and CGTase.

1994). With the assistance of surrounding amino acid residues, generating CDs that subsequently separate rapidly from the enzyme. A new amylose molecule immediately binds to the CGTase, initiating the next reaction cycle (Lin et al., 2024).

3.10.2. *Analysis of the docking mechanism between CDs and starch*

Based on the hydrogen bonding interactions and pose score results in Fig. 8 (data not reported), the binding energies of all starch glucose residues with CDs were negative, indicating that the binding between them is spontaneous (Xu et al., 2024). In amylose, the binding energies of γ-CD, β-CD, and α-CD increase sequentially (−7.1, −5.2, and − 4.4 kcal/mol), indicating that amylose residues have the highest affinity for γ-CD (Dai et al., 2024). The smaller cavity of α-CD limits its ability to encapsulate amylose residues, resulting in a lower binding energy (Fig. 8B1). In contrast, the larger cavity of γ-CD can more effectively accommodate parts of the amylose structure, enhancing hydrophobic encapsulation through the formation of multiple hydrogen bonds, thereby increasing the overall stability of the complex (Fig. 8B5). A similar trend was observed for amylopectin, where the cavity volume of γ-CD (with the lowest binding energy of −9.0 kcal/mol) was well-suited to accommodate the complex branched structure of amylopectin. It formed multiple stable hydrogen bonds, with each branch fitting into the hydrophobic cavity of γ-CD. The hydrogen bond distances between γ-CD and amylopectin residues ranged from 2.2 to 2.8 Å (Fig. 8B6). In contrast, the smaller cavity of α-CD could not fully accommodate the branched structure of amylopectin (Fig. 8B2), resulting in weaker

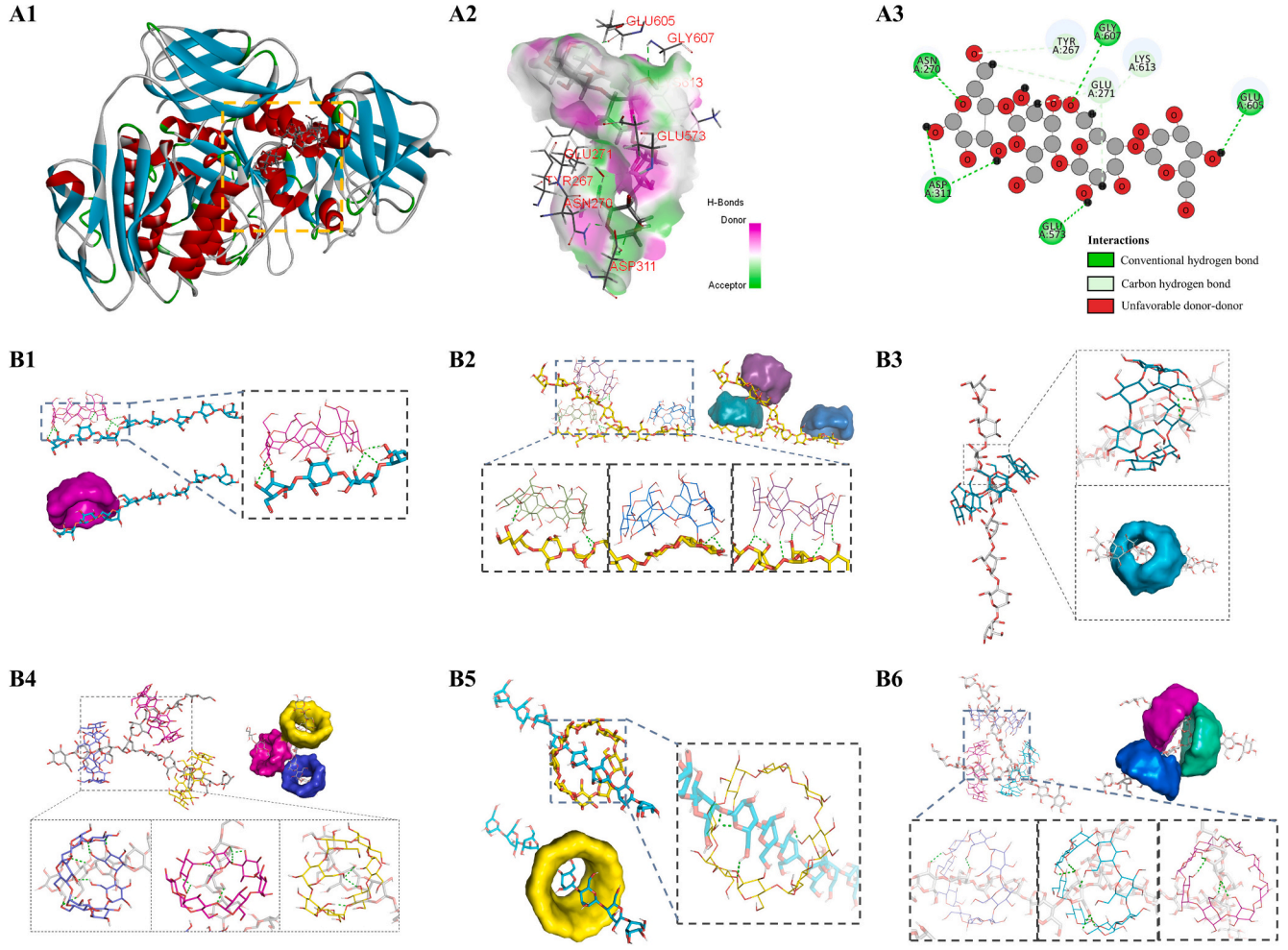

Fig. 8. Overview of the binding model between CGTase and glucose residues (A1-A3). B1-B6 represents molecular docking analysis of *α*-CD, *β*-CD, and *γ*-CD interacting with amylose and amylopectin, with dashed lines indicating hydrogen bond interactions. CGTase: Cyclodextrin glycosyltransferase; CD: Cyclodextrin.

binding and less effective hydrophobic encapsulation.

Overall, γ-CD demonstrated the tightest binding with starch residues, making it superior in enhancing the solubility, stability, and bioavailability of starch, which supports the development of novel materials with enhanced stability, solubility, and controlled-release properties. This explains the significant improvement in the resistant digestion properties of CGTase-modified starch. Fig. 8 B1-B6 show the surface forms of α-, β-, and γ-CD. The surface representation highlights the larger hydrophobic cavity and internal structural features of γ-CD, which can accommodate segments of amylose and amylopectin residues within its cavity. Through the encapsulating effect of γ-CD, starch fragments are partially protected, reducing their exposure to external factors such as enzymatic degradation (Zhang et al., 2024).

4. Conclusion

In this study, potato starch was modified through the combined effects of PAW, extrusion, and CGTase. The results demonstrated that the modification led to changes in the structural, thermal, water distribution, rheological, and digestibility properties of potato starch. PAW produced only etching effects on the starch surface, while extrusion and CGTase disrupted the internal growth ring structure. CGTase modification reduced long-chain starch content, increasing short-chain starch (DP < 6 accounted for 73.13 %), with no crystalline peaks observed. It also decreased bound water by reducing water-binding sites. The EACG-modified starch exhibited the highest thermal stability and gel modulus, making it suitable for frozen and canned food applications. *In vitro* digestion results indicated that CGTase modification, enhanced by extrusion and PAW, produced more short-chain starch and increased resistant starch from 31.69 % to 61.38 %. Molecular docking revealed that CDs produced during modification bound with starch residues through hydrogen bonds and other intermolecular forces, with γ-CD most effectively encapsulating glucose residues. This study developed a novel method for modifying potato starch using the combined technologies of PAW, extrusion, and CGTase, improving its functional, gel, and digestive properties, and supporting the development of low-GI potato-based functional foods. Future research could explore the effects of modification on final structure, safety, storage characteristics, and microbial inactivation of starch.

CRediT authorship contribution statement

Fanglei Zou: Writing – review & editing, Writing – original draft, Visualization, Methodology, Conceptualization. **Hongyun Hao:** Visualization, Software, Methodology, Conceptualization. **Miao Yang:** Writing – review & editing, Conceptualization. **Chunming Tan:** Data curation, Conceptualization. **Lin Chen:** Writing – review & editing, Methodology. **Junhua Wu:** Methodology, Investigation. **Hongying Wang:** Writing – review & editing, Supervision, Resources, Project administration, Funding acquisition.

Declaration of competing interest

The authors declare that they have no known competing financial interests or personal relationships that could have appeared to influence the work reported in this paper.

Acknowledgment

This research was supported by the National Key Research and Development Program of China (Grant number: 2021YFD1300300).

Appendix A. Supplementary data

Supplementary data to this article can be found online at https://doi.org/10.1016/j.foodchem.2025.145247.

Data availability

Data will be made available on request.

References

Ab'lah, N., Yusuf, C. Y. L., Rojsitthisak, P., & Wong, T. W. (2023). Reinvention of starch for oral drug delivery system design. *International Journal of Biological Macromolecules, 241*, Article 124506. https://doi.org/10.1016/j.ijbiomac.2023.124506

Aguado, R., Murtinho, D., & Valente, A. J. (2021). Association of antioxidant monophenolic compounds with β-cyclodextrin-functionalized cellulose and starch substrates. *Carbohydrate Polymers, 267, Article 118189*. https://doi.org/10.1016/j.carbpol.2021.118189

Akhila, P. P., Sunooj, K. V., Bangar, S. P., Aaliya, B., Navaf, M., Indumathy, B., et al. (2024). Assessing the impact of plasma-activated water-assisted heat-moisture treatment on the extrusion-recrystallization process of hausa potato starch. *Carbohydrate Polymers, 335, Article 122081*. https://doi.org/10.1016/j.carbpol.2024.122081

Ali, S., Singh, B., & Sharma, S. (2020). Effect of processing temperature on morphology, crystallinity, functional properties, and *in vitro* digestibility of extruded corn and potato starches. *Journal of Food Processing and Preservation, 44(7), Article e14531*. https://doi.org/10.1111/jfpp.14531

An, N.-N., Li, D., Wang, L.-J., & Wang, Y. (2023). Microwave irradiation of corn kernels: Effects on structural, thermal, functional and rheological properties of corn flour. *Food Hydrocolloids, 143, Article 108939*. https://doi.org/10.1016/j.foodhyd.2023.108939

Benavent-Gil, Y., Rosell, C. M., & Gilbert, E. P. (2021). Understanding CGTase action through the relationship between starch structure and cyclodextrin formation. *Food Hydrocolloids, 112, Article 106316*. https://doi.org/10.1016/j.foodhyd.2020.106316

Bloch, F. (1946). *Nuclear induction. Physical review, 70*(7–8), 460. https://doi.org/10.1103/PhysRev.70.460

Bragg, W. H., & Bragg, W. L. (1913). The reflection of X-rays by crystals. *Proceedings of the Royal Society of London. Series A, Containing Papers of a Mathematical and Physical Character, 88*(605), 428–438.

Casewit, C., Colwell, K., & Rappe, A. (1992). Application of a universal force field to organic molecules. *Journal of the American Chemical Society, 114*(25), 10035–10046. https://doi.org/10.1021/ja00051a041

Cheng, Y., Wang, B., Lv, W., Zhong, Y., & Li, G. (2024). Effect of xanthan gum on physicochemical properties and 3D printability of emulsion-filled starch gels. *Food Hydrocolloids, 149, Article 109613*. https://doi.org/10.1016/j.foodhyd.2023.109613

Chou, Y.-J., Tseng, Y.-H., Hsieh, K. C., & Ting, Y. (2023). The effect of plasma-activated water treatment on the physicochemical properties of potato starch. *Food Bioscience, 53*, Article 102613. https://doi.org/10.1016/j.fbio.2023.102613

Dai, Y., Li, X., Jin, Z., & Bai, Y. (2024). Improving cyclodextrin yield via retarding retrogradation of debranched starches during the preparation of cyclodextrin with cyclodextrin glycosyltransferase and pullulanase. *Food Bioscience, 59*, Article 104067. https://doi.org/10.1016/j.fbio.2024.104067

Daudt, R. M., Külkamp-Guerreiro, I. C., Cladera-Olivera, F., Thys, R. C. S., & Marczak, L. D. F. (2014). Determination of properties of *Pinhão* starch: Analysis of its applicability as pharmaceutical excipient. *Industrial Crops and Products, 52*, 420–429. https://doi.org/10.1016/j.indcrop.2013.10.052I

Englyst, H. N., Kingman, S., & Cummings, J. (1992). Classification and measurement of nutritionally important starch fractions. *European Journal of Clinical Nutrition, 46*, S33–S50. https://doi.org/10.1128/IAI.01649-06

Fan, M., Huang, Q., Zhong, S., Li, X., Xiong, S., Xie, J., et al. (2019). Gel properties of myofibrillar protein as affected by gelatinization and retrogradation behaviors of modified starches with different crosslinking and acetylation degrees. *Food Hydrocolloids, 96*, 604–616. https://doi.org/10.1016/j.foodhyd.2019.05.045

Gannimani, R., Perumal, A., Ramesh, M., Pillay, K., Soliman, M. E., & Govender, P. (2015). Antipyrine–gamma cyclodextrin inclusion complex: Molecular modeling, preparation, characterization and cytotoxicity studies. *Journal of Molecular Structure, 1089*, 38–47. https://doi.org/10.1016/j.molstruc.2015.02.017

Ge, X., Shen, H., Su, C., Zhang, B., Zhang, Q., Jiang, H., & Li, W. (2021). The improving effects of cold plasma on multi-scale structure, physicochemical and digestive properties of dry heated red adzuki bean starch. *Food Chemistry, 349*, Article 129159. https://doi.org/10.1016/j.foodchem.2021.129159

Han, Q., Wen, X., Gao, J., Zhong, C., & Ni, Y. (2023). Application of plasma-activated water in the food industry: A review of recent research developments. *Food Chemistry, 405*, 134797. https://doi.org/10.1016/j.foodchem.2022.134797

Hyun, K., Wilhelm, M., Klein, C. O., Cho, K. S., Nam, J. G., Ahn, K. H., et al. (2011). A review of nonlinear oscillatory shear tests: Analysis and application of large amplitude oscillatory shear (LAOS). *Progress in Polymer Science, 36*(12), 1697–1753. https://doi.org/10.1016/j.progpolymsci.2011.02.002

Ji, H., Bai, Y., Li, X., Zheng, D., Shen, Y., & Jin, Z. (2020). Structural and property characterization of corn starch modified by cyclodextrin glycosyltransferase and specific cyclodextrinase. *Carbohydrate Polymers, 237, Article 116137*. https://doi.org/10.1016/j.carbpol.2020.116137

Ji, H., Li, X., Bai, Y., Shen, Y., & Jin, Z. (2021). Synergetic modification of waxy maize starch by dual-enzyme to lower the *in vitro* digestibility through modulating molecular structure and malto-oligosaccharide content. *International Journal of Biological Macromolecules, 180*, 187–193. https://doi.org/10.1016/j.ijbiomac.2021.02.219

Knoll, M., & Ruska, E. (1932). The electron microscope. *Zeitschrift für Physik, 78*(5–6), 318–339339.

Kurdziel, M., Łabanowska, M., Pietrzyk, S., Pająk, P., Królikowska, K., & Szwengiel, A. (2022). The effect of UV-B irradiation on structural and functional properties of corn and potato starches and their components. *Carbohydrate Polymers, 289*, Article 119439. https://doi.org/10.1016/j.carbpol.2022.119439

Lawson, C. L., van Montfort, R., Strokopytov, B., Rozeboom, H. J., Kalk, K. H., de Vries, G. E., et al. (1994). Nucleotide sequence and X-ray structure of cyclodextrin glycosyltransferase from Bacillus circulans strain 251 in a maltose-dependent crystal form. *Journal of Molecular Biology, 236*(2), 590–600. https://doi.org/10.1006/jmbi.1994.1168

Leach, H. W., McCowen, L. D., & Schoch, T. J. (1959). Structure of the starch granule. I. Swelling and solubility patterns of various starches. *Cereal Chemistry, 36*, 534–544.

Li, X., Ji, H., Bai, Y., & Jin, Z. (2021). Development of pullulanase mutants to enhance starch substrate utilization for efficient production of β-CD. *International Journal of Biological Macromolecules, 168*, 640–648. https://doi.org/10.1016/j.ijbiomac.2020.11.120

Li, Y., Li, C., Gu, Z., Cheng, L., Hong, Y., & Li, Z. (2019). Digestion properties of corn starch modified by α-D-glucan branching enzyme and cyclodextrin glycosyltransferase. *Food Hydrocolloids, 89*, 534–541. https://doi.org/10.1016/j.foodhyd.2018.11.025

Li, Z., Chen, S., Gu, Z., Chen, J., & Wu, J. (2014). Alpha-cyclodextrin: Enzymatic production and food applications. *Trends in Food Science & Technology, 35*(2), 151–160. https://doi.org/10.1016/j.tifs.2013.11.005

Liang, D., Luo, H., Sun, Z., Liu, Q., Zhao, L., & Li, W. (2024). Effect of amylose partial extraction on citrate esterification of potato starch and its role in structure and physicochemical modification. *Carbohydrate Polymers, 338, Article 122208*. https://doi.org/10.1016/j.carbpol.2024.122208

Lin, R., Zang, X., Yuan, C., Yu, B., Liu, P., Fang, Y., & Cui, B. (2024). Self-growing micro/nano hexagonal cyclodextrins based on dual enzyme synergism and low-temperature induction. *Chemical Engineering Journal, 483*, Article 149392. https://doi.org/10.1016/j.cej.2024.149392

Liu, H., Xie, F., Yu, L., Chen, L., & Li, L. (2009). Thermal processing of starch-based polymers. *Progress in Polymer Science, 34*(12), 1348–1368. https://doi.org/10.1016/j.progpolymsci.2009.07.001

López-de-Dicastillo, C., Gallur, M., Catalá, R., Gavara, R., & Hernández-Muñoz, P. (2010). Immobilization of β-cyclodextrin in ethylene-vinyl alcohol copolymer for active food packaging applications. *Journal of Membrane Science, 353*, 184–191. https://doi.org/10.1016/j.memsci.2010.02.049

López-Nicolás, J. M., & García-Carmona, F. (2007). Use of cyclodextrins as secondary antioxidants to improve the color of fresh pear juice. *Journal of Agricultural and Food Chemistry, 55*(15), 6330–6338. https://doi.org/10.1021/jf070819x

Ma, J., Fan, J., Xia, Y., Kou, X., Ke, Q., & Zhao, Y. (2023). Preparation of aromatic β-cyclodextrin nano/microcapsules and corresponding aromatic textiles: A review. *Carbohydrate Polymers, 308, Article 120661*. https://doi.org/10.1016/j.carbpol.2023.120661

Mahmood, K., Kamilah, H., Shang, P. L., Sulaiman, S., Ariffin, F., & Alias, A. K. (2017). A review: Interaction of starch/non-starch hydrocolloid blending and the recent food applications. *Food Bioscience, 19*, 110–120. https://doi.org/10.1016/j.fbio.2017.05.006

Parker, R., & Ring, S. G. (2001). Aspects of the physical chemistry of starch. *Journal of Cereal Science, 34*(1), 1–17. https://doi.org/10.1006/jcrs.2000.0402

Román, L., Dura, Á., Martínez, M. M., Rosell, C. M., & Gómez, M. (2016). Combination of extrusion and cyclodextrin glucanotransferase treatment to modify wheat flours functionality. *Food Chemistry, 199*, 287–295. https://doi.org/10.1016/j.foodchem.2015.12.040

Roman, L., Gomez, M., Hamaker, B. R., & Martinez, M. M. (2018). Shear scission through extrusion diminishes inter-molecular interactions of starch molecules during storage. *Journal of Food Engineering, 238*, 134–140. https://doi.org/10.1016/j.jfoodeng.2018.06.019

Singh, N., Isono, N., Srichuwong, S., Noda, T., & Nishinari, K. (2008). Structural, thermal and viscoelastic properties of potato starches. *Food Hydrocolloids, 22*(6), 979–988. https://doi.org/10.1016/j.foodhyd.2007.05.010

Srangsomjit, N., Bovornratanaraks, T., Chotineeranat, S., & Anuntagool, J. (2022). Solid-state modification of tapioca starch using atmospheric nonthermal dielectric barrier discharge argon and helium plasma. *Food Research International, 162, Article 111961*. https://doi.org/10.1016/j.foodres.2022.111961

Su, C., Saleh, A. S., Zhang, B., Zhao, K., Ge, X., Zhang, Q., & Li, W. (2020). Changes in structural, physicochemical, and digestive properties of normal and waxy wheat starch during repeated and continuous annealing. *Carbohydrate Polymers, 247, Article 116675*. https://doi.org/10.1016/j.carbpol.2020.116675

Sun, X., Sun, Z., Guo, Y., Zhao, J., Zhao, J., Ge, X., et al. (2021). Effect of twin-xuscrew extrusion combined with cold plasma on multi-scale structure, physicochemical properties, and digestibility of potato starches. *Innovative Food Science & Emerging Technologies, 74, Article 102855*. https://doi.org/10.1016/j.ifset.2021.102855

Trott, O., & Olson, A. J. (2010). AutoDock Vina: Improving the speed and accuracy of docking with a new scoring function, efficient optimization, and multithreading. *Journal of Computational Chemistry, 31*(2), 455–461. https://doi.org/10.1002/jcc.21334

van der Veen, B. A., van Alebeek, G. J. W., Uitdehaag, J. C., Dijkstra, B. W., & Dijkhuizen, L. (2000). The three transglycosylation reactions catalyzed by cyclodextrin glycosyltransferase from Bacillus circulans (strain 251) proceed via different kinetic mechanisms. *European Journal of Biochemistry, 267*(3), 658–665. https://doi.org/10.1046/j.1432-1327.2000.01031.x

Wang, L., Wang, M., Zhou, Y., Wu, Y., & Ouyang, J. (2022). Influence of ultrasound and microwave treatments on the structural and thermal properties of normal maize starch and potato starch: A comparative study. *Food Chemistry, 377*, Article 131990. https://doi.org/10.1016/j.foodchem.2021.131990

Watson, E., O'neill, M., Justin, J., & Brenner, N. (1964). A differential scanning calorimeter for quantitative differential thermal analysis. *Analytical Chemistry, 36*(7), 1233–1238.

Wei, W., Wu, M., Ren, W., Yu, H., & Sun, D. (2024). Preparation of crosslinked starches with enhanced and tunable gel properties by the cooperative crosslinking-extrusion combined modification. *Carbohydrate Polymers, 324, Article 121473*. https://doi.org/10.1016/j.carbpol.2023.121473

Wu, C., Sun, R., Zhang, Q., & Zhong, G. (2020). Synthesis and characterization of citric acid esterified canna starch (RS4) by semi-dry method using vacuum-microwave-infrared assistance. *Carbohydrate Polymers, 250, Article 116985*. https://doi.org/10.1016/j.carbpol.2020.116985

Wu, H., Li, X., Ji, H., Svensson, B., & Bai, Y. (2022). Improved production of gamma-cyclodextrin from high-concentrated starch using enzyme pretreatment under swelling condition. *Carbohydrate Polymers, 284*, Article 119124. https://doi.org/10.1016/j.carbpol.2022.119124

Xie, Y., Yan, M., Yuan, S., Sun, S., & Huo, Q. (2013). Effect of microwave treatment on the physicochemical properties of potato starch granules. *Chemistry Central Journal, 7*(113). https://doi.org/10.1186/1752-153x-7-113

Xu, H., Sutar, P. P., Ren, W., & Wu, M. (2024). Revealing the mechanism of post-harvest processing on rose quality based on dynamic changes in water content, enzyme activity, volatile and non-volatile metabolites. *Food Chemistry, 448*, Article 139202. https://doi.org/10.1016/j.foodchem.2024.139202

Yan, Y., Zhu, X., Hao, M., Ji, X., Shi, M., & Niu, B. (2024). Understanding the multi-scale structure, physicochemical and digestive properties of extruded yam starch with plasma-activated water. *International Journal of Biological Macromolecules, 254*, Article 128054. https://doi.org/10.1016/j.ijbiomac.2023.128054

Yu, H.-Z., Chi, S.-Y., Li, D., Wang, L.-J., & Wang, Y. (2022). Effect of gums on the multi-scale characteristics and 3D printing performance of potato starch gel. *Innovative Food Science & Emerging Technologies, 80*, Article 103102. https://doi.org/10.1016/j.ifset.2022.103102

Zeng, X., Zheng, B., Xiao, G., & Chen, L. (2022). Synergistic effect of extrusion and polyphenol molecular interaction on the short/long-term retrogradation properties of chestnut starch. *Carbohydrate Polymers, 276, Article 118731*. https://doi.org/10.1016/j.carbpol.2021.118731

Zhang, Z., Niu, J., Wang, J., Zheng, Q., Miao, W., Lin, Q., et al. (2024). Advances in the preparation and application of cyclodextrin derivatives in food and the related fields. *Food Research International, 195*, Article 114952. https://doi.org/10.1016/j.foodres.2024.114952

Zheng, L.-Y., Li, D., Wang, L.-J., & Wang, Y. (2024). Tailoring 3D-printed high internal phase emulsion-rice starch gels: Role of amylose in rheology and bioactive stability. *Carbohydrate Polymers, 331, Article 121891*. https://doi.org/10.1016/j.carbpol.2024.121891

Zhong, Y., Zeng, S., Lv, Y., Lv, W., Xiao, H., & Sheng, S. (2024). Effect of guar gum on the rheological properties, microstructure and 3D printing performance of egg yolk powder-potato starch composite gel. *Food Hydrocolloids, 153*, Article 110018. https://doi.org/10.1016/j.foodhyd.2024.110018

Zhou, C. Y., Wu, M., Sun, D. Y., Wei, W. G., Yu, H. Z., & Zhang, T. (2022). Twin-screw extrusion of oat: Evolutions of rheological behavior, thermal properties and structures of extruded oat in different extrusion zones. *Foods, 11*(15). https://doi.org/10.3390/foods11152206

Zhuang, Y., Wang, Y., & Yang, H. (2023). Characterizing digestibility of potato starch with cations by SEM, X-ray, LF-NMR, FTIR. *Food Chemistry, 424, Article 136396*. https://doi.org/10.1016/j.foodchem.2023.136396

Zou, F., Shinali, T. S., Yang, M., Zhong, Y., Wu, J., Wang, L., et al. (2024). Incorporation of ascorbic acid in chitosan-based coating combined with plasma-activated water: A technology for quality preservation of red grapes after simulated transportation. *International Journal of Biological Macromolecules, 270, Article 132366*. https://doi.org/10.1016/j.ijbiomac.2024.132366

Zou, F., Tan, C., Chang, Z., Shinali, T. S., Zhang, B., Zhang, L., et al. (2024). New strategy for improving postharvest quality of cherry tomatoes: Synergy of plasma-activated water and welsh onion leaf protein extracts. *Food Control, 164, Article 110592*. https://doi.org/10.1016/j.foodcont.2024.110592

Zou, F., Yang, M., Wu, J., Wang, L., & Wang, H. (2025). The potential of plasma-activated water in safe and sustainable food production: A comprehensive review of recent advances and future trends. *Critical Reviews in Food Science and Nutrition, 1–25*. https://doi.org/10.1080/10408398.2025.2477799

Zou, F., Zuo, Y., Tan, C., Yang, M., Wang, L., & Wang, H. (2024). Structural, physicochemical, functional, and digestive properties of corn flour modified by plasma-activated water combined with hydrothermal treatments. *LWT, 210*, 116858. https://doi.org/10.1016/j.lwt.2024.116858

Zuo, Y., Zou, F., Yang, M., Xu, G., Wu, J., Wang, L., et al. (2024). Effects of plasma-activated water combined with ultrasonic treatment of corn starch on structural, thermal, physicochemical, functional, and pasting properties. *Ultrasonics Sonochemistry, 108, Article 106963*. https://doi.org/10.1016/j.ultsonch.2024.106963